 CMES, vol.99, no.3, pp.195-208, 2014

Large Eddy Simulation of Three Dimensional Impinging Jets

Nadjib Ghiti[1]

Abstract: This paper presents a large eddy simulation of three dimensional vertically impinging jet on a horizontal plate. The air impinging jet was simulated using the perturbed method based on a high vortex number in the jet inlet for different ranges of Reynolds number Re= 6000, 8000, 10000, 12000, 14000 and for the same distance between the jet and the impinging plate. The effect of the Reynolds number of the air jet impinging on a horizontal plate was studied; the study showed that the vorticity magnitude is increased with the increasing of the Reynolds number. The turbulent flow jet was decomposed into three principal regions: the free jet region, the impinging point region and the wall jet region. The increase of the jet Reynolds number has a strong effect on the turbulent characteristics of the flow near the wall plate.

Keywords: Large eddy simulation, impinging jet, turbulence, Reynolds number.

Nomenclature

$\bar{\varphi}$	Filtered variable
x, x'	variables
D	fluid domain
G	filter function
V	volume of a computational cell
G(x, x')	filter function
σ_{ij}	stress tensor
τ_{ij}	sub-grid scale stress
μ_t	sub-grid scale turbulent viscosity
$\bar{S}_{ij}$	rate-of-strain tensor
T_{ij}	The compressible form of the Sub-grid stress tensor

[1] Corresponding Author. Doctor in Mechanical Engineering and Trainer at Petrofac Training services UAE. Tel.: +213 551 77 45 68; fax: +213 21 20 77 65. Email: ghitinadjib@gmail.com , ghitinadjib@yahoo.fr

ρ	Density
$\bar{u}_i$	Mean velocity
t	Time
p	Pessure
μ	Dynamic viscosity
δ_{ij}	Kroniker Delta
S^d_{ij}	Mean rate-of-strain tensor
C_W	WALE model constant
T_{ll}	Term added to a filter pressure
M_{sgs}	subgrid Mach number

1 Introduction

Impinging jets are used for several industrial applications. Jet impingement is a common concern for aerodynamicists dealing with VSTOL aircraft. The ground impingement of single or multiple jets and the influence of up wash fountains on ground based structures during takeoff operation are challenging topics of research. Impinging jets are also used for heating, cooling and drying of impingement surfaces. The jets emanate from the nozzles as laminar, but the evolution of instability and the eventual transition to turbulence take place a little distance downstream of the orifice, see Becker and Massaro (1968). For a round jet, a stagnation point is formed at the center on the impingement surface Gutmark and Wolfshtein and Wynanski (1978). The flow develops along the impingement surface in the form of a wall jet. In the stagnation zone, the strong acceleration keeps the boundary laminar Martin, H. (1977). A second transition is usually brought about immediately after the jet is transformed near the wall into a decelerated wall jet. The heat or mass transfer rate at the stagnation point is very high. Away from the stagnation point, a rapid variation of heat transfer is observed. In the case of a second transition another peak in transport rate is attained Martin, H. (1977), Gardon and Akfirat (1965) observed that the level of turbulence in the jet had a strong influence on the rate of heat transfer from the impingement plate. They deployed slot jets impinging on a flat plate. Donaldson and Snedekar and Margolis (1971) used a round jet and found that the heat transfer characteristics, away from the stagnation point, are similar to a normal turbulent boundary layer in an external flow having a free stream velocity equal to the local maximum velocity in the wall jet. In case of the plane impinging jet (which is sometimes called Hiemenz flow), Sutera and Maeder and Kestin (1963), Sutera (1965) proposed that the high heat transfer is caused by the stretched vortex aligned parallel to the wall. Yokobori and Kasagi and Hirata (1983) studied the plane impinging jet experimentally using a flow visualization

technique and observed counter-rotating vortex pairs along the wall.

Sakakibara and Hishida and Maeda (1997), Sakakibara and Hishida and Phillips (2001) Further studied the plane impinging jet using simultaneous measurements of velocity and temperature fields by digital particle image velocimetry (PIV) and laser-induced fluorescence (LIF) and found that the counter-rotating vortex pairs are convected from an upstream location and stretched in the vicinity of the wall. Andreopoulos and Rodi (1984) used a triple wire probe to simultaneously measure all three components of velocity. Kelso and Lim and Perry (1996) studied the structure of round jets in cross-flows using flow visualization techniques and flying-hot-wire measurements. This article simulates around turbulent air jet flow by means of an LES model in three dimensional coordinates system. To study the effect of Reynolds number on the flow structure near the impingement surface.

Menow and Rizk (1996) study the effect of axisymmetric and azimuthal perturbations at the jet exit for a vertical takeoff and landing aircraft. They observed that the vertical structures formed in the jet shear layer due to azimuthal forcing, show significant three dimensional vortex stretching effects when compared to the structures formed in the axisymmetric forcing. The numerical work of Jing-yu FAN and Yan ZHANG and Dao-zeng WANG (2007), to study the vertical structures for an impinging transverse jet using a large eddy simulation. They found that the scarf vortex wrapped around the impinging jet in the near wall zone showed distinct asymmetric with regard to its bilateral spiral legs within the near region. Another investigation on the plane turbulent impinging jet using a large eddy simulation by Francois and Stephane (2001) the using a spectral analysis show that the presence of contra rotative vortices near the impingement zone underlines the complexity of the flow.

The supersonic flow was studied by Dauptain and Cuenot and Gicquel (2011) using a large eddy simulation for the case of a turbulent jet impinging on a flat plate. In this study they used a very high mesh refinement to ensure the accuracy with the experimental results.

The flow field of plane impinging jets at moderate Reynolds numbers has been computed using large eddy simulation technique by Beaubert and Viazzo (2003). Two Reynolds numbers (Re =3000 and 7500) defined by the jet exit conditions are considered. The dynamics of the jet are explored using the instantaneous velocity, vorticity and low pressure fields with a focus on the impingement zone. The effect of the jet Reynolds number is significantly between 3000 and 7500 both on the near and far field structure. Unsteady phenomena linked to turbulence are best addressed with LES, which provides time-dependent filtered quantities of one flow realization. LES has been used with success to reproduce the intermittent and unsteady tone-producing modes of free jets Berland and Bogey and Bailly (2007)

and cavities Larcheveque and Sagaut and Le and Comte (2004). Combined with advanced diagnostics to take advantage of the spatial and temporal description of the problem, LES can provide specific information about non-linear interactions or causality of phenomena Chacko and Chung and Choi and Nam and Jeong (2011) Applied a large eddy simulation technique to predict the temperature fluctuations of thermal striping observed in a triple jet. The large amplitude of the temperature fluctuations associated with the thermal stripping was captured correctly.

2 Mathematical Model

The following sections give details on the governing equations for LES, the subgrid-scale turbulence models, and the boundary conditions.

2.1 Filtered Navier-Stokes Equations

The governing equations used for the LES are obtained by filtering the time-dependent Navier-Stokes equations in either Fourier (wave-number) space or configuration (physical) space. The filtering process effectively filters out the eddies whose s-cales are smaller than the filter width or grid spacing used in the computations. The resulting equations thus govern the dynamics of large eddies.

A filtered variable, denoted by an over bar, is defined by

$$\bar{\varphi} = \int_D \bar{\varphi}\left(x'\right) G\left(x,x'\right) dx' \tag{1}$$

D is the fluid domain and G is the filter function that determines the scale of the resolved eddies.

In Fluent, the finite-volume discretization itself implicitly provides the filtering op-eration

$$\bar{\varphi}\left(x\right) = \frac{1}{v}\int_v \varphi\left(x'\right) dx',\ x' \in v \tag{2}$$

V is the volume of a computational cell. The filter function G(x, x') implied here is then

$$G\left(x,x'\right)\begin{cases} \frac{1}{v}, & x' \in v \\ 0,x' & otherwise \end{cases} \tag{3}$$

The LES capability in Fluent is applicable to compressible flows. For the sake of concise notation, however, the theory is presented here for incompressible flows.

Filtering the Navier-Stokes equations, one obtains

$$\frac{\partial \rho}{\partial t} + \frac{\partial}{\partial x_i}\left(\rho \bar{u}_i\right) = 0 \tag{4}$$

And

$$\frac{\partial(\rho\bar{u}_i)}{\partial t}+\frac{\partial}{\partial x_j}(\rho\bar{u}_i\bar{u}_j)=\frac{\partial}{\partial x_j}\left(\mu\frac{\partial\sigma_{ij}}{\partial x_j}\right)-\frac{\partial\bar{p}}{\partial x_i}-\frac{\partial\tau_{ij}}{\partial x_j} \tag{5}$$

σ_{ij} is the stress tensor due to molecular viscosity by:

$$\sigma_{ij}\equiv\left[\mu\left(\frac{\partial\bar{u}_i}{\partial x_j}+\frac{\partial\bar{u}_j}{\partial x_i}\right)\right]-2/3\mu\frac{\partial\bar{u}_l}{\partial x_l}\delta_{ij} \tag{6}$$

τ_{ij} is the subgrid scale stress defined by

$$\tau_{ij}=\rho\overline{u_iu_j}-\rho\overline{u_i}\,\overline{u_j} \tag{7}$$

2.2 Subgrid-Scale Models

The subgrid-scale stresses resulting from the filtering operation are unknown, and they require modeling. The subgrid-scale turbulence models in Fluent employ the Boussinesq hypothesis Hinze (1975) as in the RANS models, computing subgrid-scale turbulent stresses from

$$\tau_{ij}-\frac{1}{3}\tau_{kk}\delta_{ij}=-2\mu_t\overline{S_{ij}} \tag{8}$$

μ_t is the subgrid-scale turbulent viscosity. The isotropic part of the subgrid-scale stresses τ_{kk} is not modeled, but added to the filtered static pressure term. $\overline{S_{ij}}$ is the rate-of-strain tensor for the resolved scale defined by

$$\overline{S_{ij}}\equiv\frac{1}{2}\left(\frac{\partial\overline{u_i}}{\partial x_j}+\frac{\partial\overline{u_j}}{\partial x_i}\right) \tag{9}$$

For compressible flows, it is convenient to introduce the density-weighted (or Favre) filtering operator

$$\varphi=\frac{\overline{\rho\varphi}}{\bar{\rho}} \tag{10}$$

The Favre Filtered Navier-Stokes equation takes the same form as Equation 5. The compressible form of the subgrid stress tensor is defined as

$$T_{ij}=-\rho u_iu_j+\bar{\rho}u_iu_j \tag{11}$$

This term is split into its isotropic and deviatoric parts

$$T_{ij}=\left(T_{ij}-\frac{1}{3}T_{ll}\delta_{ij}\right)+\frac{1}{3}T_{ll}\delta_{ij} \tag{12}$$

Such as

$T_{ij} - \frac{1}{3}T_{ll}\delta_{ij}$ deviatoric term

$\frac{1}{3}T_{ll}\delta_{ij}$ isotropic term

The deviatoric part (the first two terms) of the subgrid-scale stress tensor is modeled using the compressible form of the Smagorinsky model:

$$T_{ij} - \frac{1}{3}T_{ll}\delta_{ij} = 2\mu_t\left(\delta_{ij} - \frac{1}{3}\delta_{ii}\delta_{ij}\right) \tag{13}$$

$T_{ll} = \gamma M_{sgs}^2 \bar{p}$

The term involving T_{ll} can be added to the filtered pressure or simply neglected. This subgrid Mach number can be expected to be small when the turbulent Mach number of the flow is small.

2.2.1 Wall-Adapting Local Eddy-Viscosity (WALE) Model

In the WALE model Fluent (2006), the eddy viscosity is modeled by

$$\mu_t = \rho L_s^2 \frac{\left(S_{ij}^d S_{ij}^d\right)^{3/2}}{\left(\overline{S_{ij}S_{ij}}\right)^{5/2} + \left(S_{ij}^d S_{ij}^d\right)^{5/4}} \tag{14}$$

Ls and S_{ij}^d in the WALE model are defined, respectively, as

$$L_s = \min\left(kd, C_w V^{\frac{1}{8}}\right) \tag{15}$$

$$S_{ij}^d = \frac{1}{2\left(\overline{g_{ij}^2} + \overline{g_{ij}^2}\right)} - \frac{1}{3\delta_{ij}\overline{g_{ij}^2}},\ \overline{g_{ij}} = \frac{\partial \overline{u_i}}{\partial x_j} \tag{16}$$

In Fluent, the default value of the WALE constant, C_w, is 0.325 and it has been found to yield satisfactory results for a wide range of flow. The rest of the notation is the same as for the Smagorinsky-Lilly model. With this spatial operator, the WALE model is designed to return the correct wall asymptotic (y^3) behavior for wall bounded flows Fluent (2006).

3 Computational Domain

Using a 3D model, the impingement surface is perpendicular to the air jet; and the jet is spreading vertically on the impinging plate. The diameter of the jet is d=4 mm, Fig. 1. A large eddy simulation with the turbulent smagorinsky sub-grid scale model implemented in the CFD package is used **Fluent** (2006). The time step size is 0.01 to ensure that the simulation can capture all the behavior of the impinging jet near the impingement plate. The distance from the jet exit and the impinging wall is 12 times the jet diameter and 25 times the jet diameter to the diameter of the impinging plate. The solution convergence is determined by two criteria. The first criterion is to ensure that the residuals of the solved equations drop below specify thresholds set at 10^{-3} for all variables. The second one is to ensure that the velocity fields of the jet take the same behavior when the time step increases and spatial location is stable and is no longer changing with iterations.

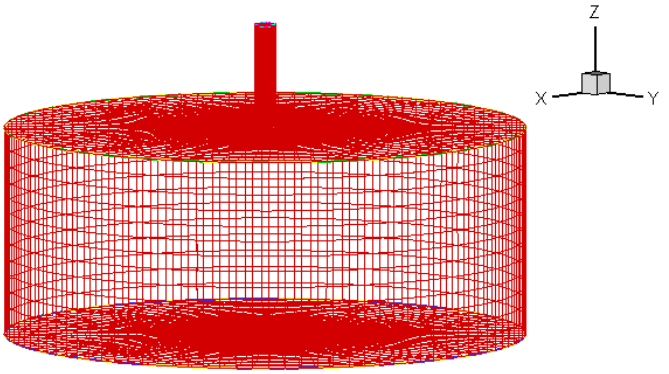

Figure 1: Schematic of mesh and frontier of physical calculation domain.

4 Numerical Results

The difference in the eddy structures in the stagnation region can be explained by the difference in the stretching directions between plane and round jets on a wall. In the case of the round jet, strong stretching is caused in the transverse direction (x-direction) by the acceleration of the flow after impingement due to the high pressure in the stagnation region, as well as by the counter-rotating roll-up eddies moving apart across the stagnation line after impingement, while little stretching or shrinking occurs in the span wise direction, Fig. 2

Therefore, a small transverse perturbation imposed upstream of the jet is strongly intensified in the stagnation region and twin vortices are produced Fig.3 In the

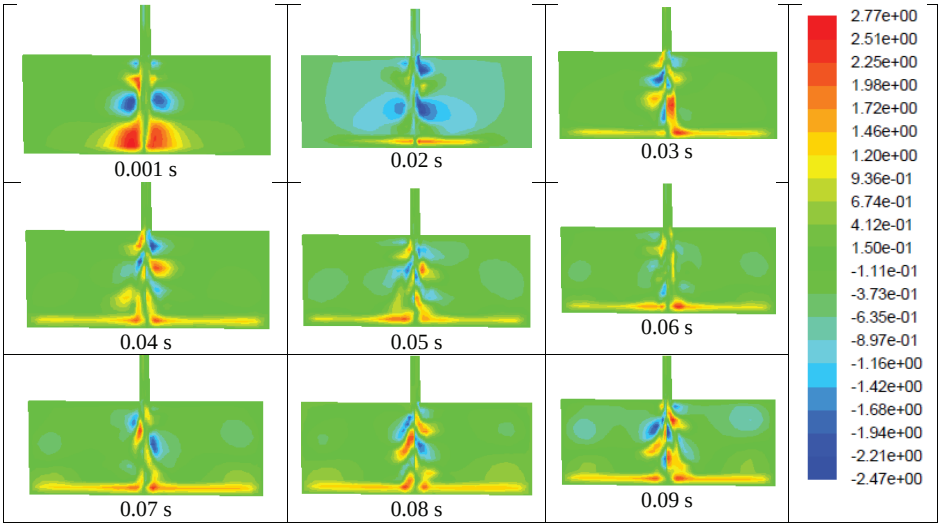

Figure 2: Contours of instantaneous radial velocity (m/s) for impinging air jet, Re=6000.

case of the round jet, the flow does not accelerate much in the r direction because of the expansion of the flow field after the impingement and azimuthal stretching dominates the flow field. The dependence of the eddy structures on the Reynolds number of the round impinging jet is investigated here with the characteristic twin vortices in the stagnation region of round jets being of main concern. Accordingly the higher Reynolds number case of 14000 is studied using LES in this section. The accuracy of LES in the round jet is demonstrated by comparisons with experimental data in Tsubokura and Kobayashi and Taniguchi (1997). The flow-fields in the stagnation region at higher Reynolds numbers also show less organized and coherent structure than the ones at the low Reynolds number. Fig.6a shows instantaneous velocity vectors for Reynolds number of 8000 at the y=0 plane. The jet shows a laminar structure at the exit and the laminar regime continues for a short distance downstream. When y = 6d, the unstable laminar shear layers begin to break down the vortices. In the figure, these vortices and the motion of the individual vortices has been examined as they move along the surface and out of the domain of interest. The flow shows somewhat steady character near the impingement point. After the impingement, the jet forms into two wall jets on the surface. Entrainment from the upper part of the domain is induced by vortices wrapping the ambient fluid about them.

Fig. 3(a ,b) shows an axisymmetric instantaneous velocity vectors of an impinging

jet for Reynolds number of 8000 on (x-y) plane. Three regions appear:

The free jet region

The wall jet region

The potential core region.

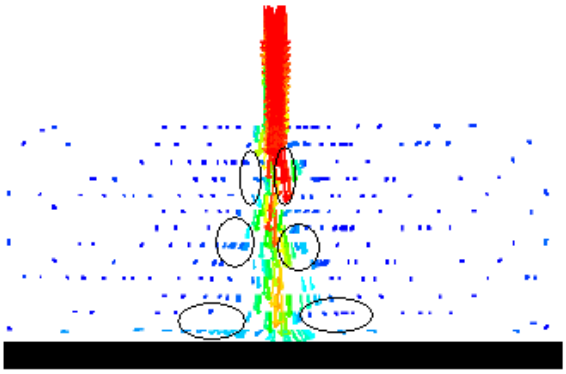

Figure 3a: Instantaneous velocity vectors on x-y plane for Re= 8000.

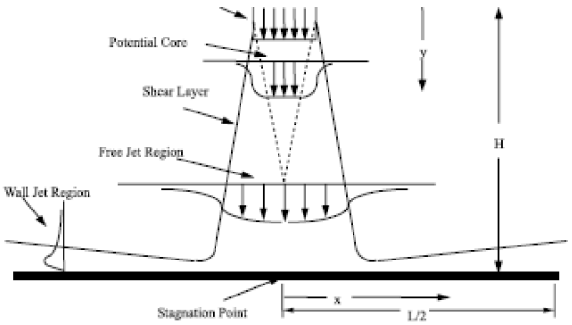

Figure 3b: The three regions in an impinging jet.

In the Fig. 4 the contours of instantaneous velocity magnitude in different time instances for the low Reynolds number show the jet wall impingement structure development from time to time. In the first instance 0.001second the jet is not influenced by the wall that is not arrived yet to the wall, the jet impingement is fully developed at 0.09 second and influenced by the impinging wall. Fig. 5 Shown five different cases are computed to clarify the possible influence of the jet Reynolds number. The Reynolds number $Re = \frac{v.d}{v}$ is set to 6000 for case (I), 8000 for

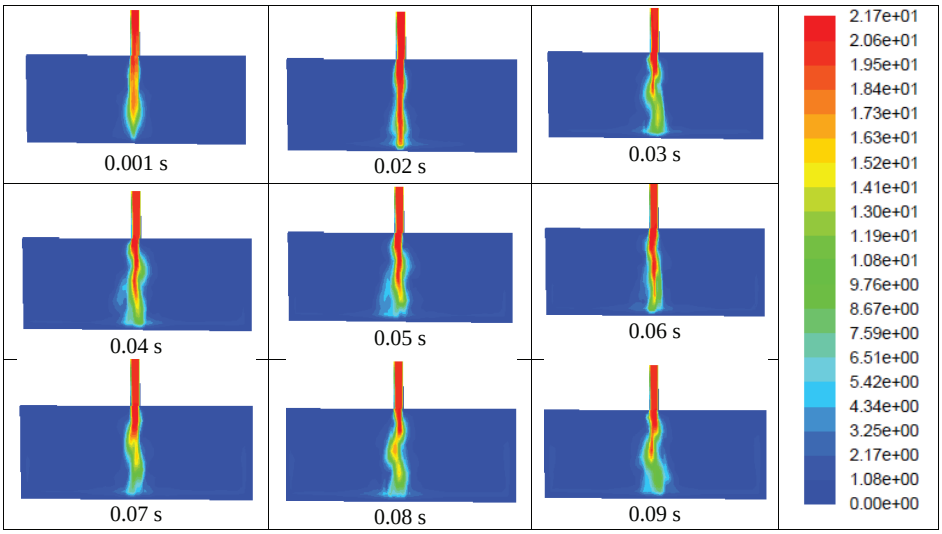

Figure 4: Contours of instantaneous velocity magnitude (m/s) for impinging air jet, Re=6000.

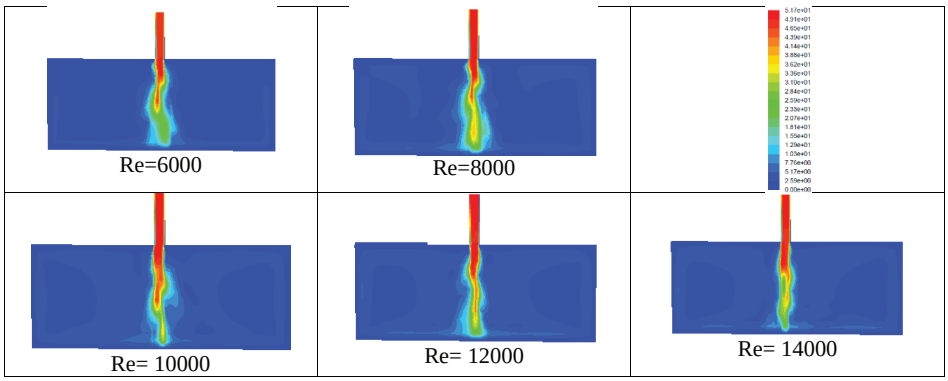

Figure 5: Contours of the instantaneous velocity magnitude at the same instance for different Reynolds number, t = 1 second.

case (II) and 10000 for case (III), 12000 for case (IV), 14000 for case (VI). The nondimensional time step $\frac{\Delta t.V}{d}$ is fixed to a value which ensures the stability of the numerical scheme (CFL $<$ 0.3). For the largest Reynolds number simulation (Re =14000), we have to mention that only first order statistics are here reported since insufficient integration times are yet available for this case. The dynamics of the impinging jet are explored using the instantaneous velocity, vorticity and low pres-

sure fields, the effect of the Reynolds number of the flow structure is also studied. Fig. 6 show the Sub grid scale viscosity ratio (a), and Sub-grid scale dynamic viscosity constant (b) from the two contours the effect of viscosity on the turbulent impinging jet is clear near the impingement point when a strong strain rate of the vortices is existed.

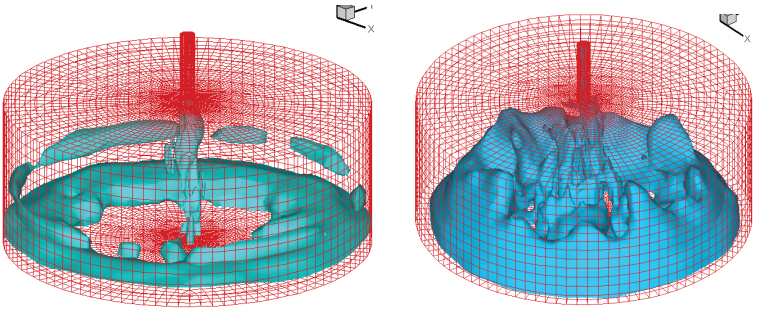

(a) (b)

Figure 6: Sub grid scale viscosity ratio (a), Sub-grid scale dynamic viscosity constant (b).

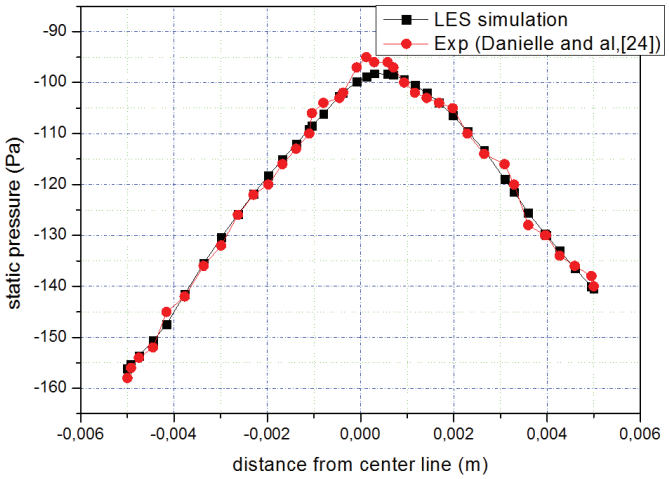

Figure 7: Radial pressure distributions of the jet.

The radial pressure distribution on the impingement surface Fig. 7 shows a good agreement with the experimental data obtained by Danielle and Guerra and Atila

and Silva (2005) [24], the pick of high pressure values is centered in the middle of impinging point where a strong effect of the jet momentum defined by the axial velocity. When the turbulent jet deflected on the impinging plate, a wall jet region was created and permit to the flow spread in the radial direction with decreasing in pressure.

5 Conclusion

The present simulations of a 3 dimensional turbulent impinging jets enable the study of the dynamics of the vortices which is difficult to reach in experiments. They are also intended to develop a better understanding of three impinging jet physics to help derive physically accurate results of turbulent vortices' structures near the impinging plate.

The influence of the Reynolds number on the jet development appears to be well reproduced in the LES using the filtering alone.

References

Andreopoulos, J.; Rodi, W. (1984): Experimental investigations of jets in a cross-flow. *Journal of Fluid Mechanics,* vol. 138, pp. 93–127.

Beaubert, F.; Viazzo. S. (2003): Large eddy simulations of plane turbulent impinging jets at moderate Reynolds numbers. *International Journal of Heat and Fluid Flow,* vol. 24, pp. 512–519.

Becker, H. A.; Massaro, T. A. (1968): Vortex evolution of a round jet. *J. Fluid Mech.*, vol. 31, pp. 435-448.

Berland, J.; Bogey, C.; and Bailly, C. (2007): Numerical study of screech generation in a planar supersonic jet. *Phys. Fluids* vol. 19, pp. 075105.

Chacko, S.; Chung, Y. M.; Choi, S. K.; Nam, H. Y.; Jeong, H. Y. (2011): Large-eddy simulation of striping in unsteady non-isothermal triple jet. *International Journal of Heat and Mass Transfer*, vol. 55 pp. 4400-4409.

Danielle, R. S.; Guerra, J. S.; Atila, P.; Silva, F. (2005): The near wall behavior of an impinging jet. *International Journal of Heat and Mass Transfer,* vol. 48, pp. 2829–2840.

Dauptain, A.; Cuenot, B.; Gicquel, L. Y. M. (2011): Large Eddy Simulation of a Stable Supersonic Jet Impinging on a Flat Plate. 42 ave. G. Coriolis 31057 Toulouse – France

Donaldson, C. B.; Snedekar, R. S.; Margolis, D. P. (1971): A study of free jet turbulent structure and impingement heat transfer. *J. Fluid Mech.,* vol. 45, pp. 477-512.

Fan, J.; Zhang, Y.; Wang, D. (2007): Large-eddy simulation of three-dimensional vortical structures for an impinging transverse jet in the near region. *Journal of Hydrodynamics,* Ser. B vol. 19, Issue 3, pp. 314–321.

Francois, B.; Stephane, V. (2001): Large Eddy Simulations of Plane Turbulent Impinging Jets. *14th Australasian Fluid Mechanics Conference Adelaide University*, Adelaide, Australia pp. 10-14.

Fluent 6.3. (2006): User's Guide, Fluent Inc. Centerra Resource Park 10 Cavendish Court Lebanon, NH 03766.

Hinze, J. O. (1975): Turbulence. *McGraw-Hill Publishing Co*., New York.

Gardon, R.; Akfirat, J. C. (1965): The role of turbulence in determining the heat transfer characteristics of impinging jets. *Int. J. Heat Mass Transfer,* vol. 8, pp. 1261-1272.

Gutmark, E.; Wolfshtein, M.; Wynanski, I. (1978): The plane turbulent impinging jet. *J. Fluid Mech*., vol. 88, pp. 737-756.

Kelso, R.; Lim, T.; Perry, A. (1996): An experimental study of round jets in cross-flow. *Journal of Fluid Mechanics,* vol. 306, pp. 111–144.

Larcheveque, L.; Sagaut, P.; Le, T.; Comte, P. (2004) "Large-eddy simulation of a compressible flow in a three-dimensional open cavity at high Reynolds number. *J. Fluid Mech.,* vol. 516, pp. 265–301.

Martin, H. (1977): Heat and mass transfer between impinging gas jets and solid surface. In: Hartnett, J.P., Irvine, T.F. (Eds.), *Advances in Heat Transfer*, vol. 13, pp. 1-60.

Menow, S.; Rizk, M. (1996): Large-Eddy Simulations of Forced Three-Dimensional Impinging Jets. *International Journal of Computational Fluid Dynamics*, vol. 7, issue 3, pp. 275-289.

Sutera, S. P.; Maeder, P. F.; Kestin, J. (1963): On the sensitivity of heat transfer in the stagnation-point boundary layer to free-stream vorticity. *J. Fluid Mech.,* vol. 16, pp. 497–520.

Sutera, S. P. (1965): Vorticity amplification in stagnation-point flow and its effect on heat transfer. *J. Fluid Mech.,* vol. 21, no 3, pp. 513–534.

Sakakibara, J.; Hishida, K.; Maeda, M. (1997): Vortex structure and heat transfer in the stagnation region of an impinging plane jet. *Int. J. Heat Mass Transfer,* vol. 40, no 13, pp. 3163–3176.

Sakakibara, J.; Hishida, K.; Phillips, R. C. (2001): On the vertical structure in a plane impinging jet. *J. Fluid Mech.,* vol. 434, pp. 273–300.

Tsubokura, M.; Kobayashi, T.; Taniguchi, N. (1997): Large eddy simulation of

plane impinging jets. *Proc. 11th Symp. on Turbulent Shear Flow,* Grenoble, pp. 2224–2229.

Yokobori, S.; Kasagi, N.; Hirata, M.; (1983): Transport phenomena at the stagnation region of a two-dimensional impinging jet. *Trans. JSME,* ser. B 49, no 441, pp. 1029–1039.